

# Accurate Transient Calorimetric Measurement of Soft-Switching Losses of 10-kV SiC MOSFETs and Diodes

Daniel Rothmund<sup>✉</sup>, Student Member, IEEE, Dominik Bortis, Member, IEEE,  
and Johann Walter Kolar<sup>✉</sup>, Fellow, IEEE

**Abstract**—The characterization of soft-switching losses (SSL) of modern high-voltage SiC MOSFETs is a difficult but necessary task in order to provide a sound basis for the accurate modeling of converter systems, such as medium-voltage-connected solid-state transformers, where soft-switching techniques are employed to achieve an improved converter efficiency. Switching losses (SL), in general, are typically measured with the well-known double pulse method. In the case of SSL measurements, however, this method is very sensitive to the limited accuracy of the measurement of the current and voltage transients, and thus is unsuitable for the characterization of fast-switching high-voltage MOSFETs. This paper presents an accurate and reliable calorimetric method for the determination of SSL using the example of 10-kV SiC MOSFET modules. Measured SSL curves are presented for different dc-link voltages and switched currents. Furthermore, a deeper analysis concerning the origin of SSL is performed. With the proposed measurement method, it can be experimentally proven that the largest share of the SSL arises from charging and discharging the output capacitance of the MOSFET module and especially of the antiparallel junction barrier Schottky diode.

**Index Terms**—Calorimetric measurement, junction barrier Schottky (JBS) diode, soft-switching losses, zero voltage switching (ZVS), 10-kV SiC MOSFETs.

## I. INTRODUCTION

SOFT-SWITCHING techniques are widely used in power electronic converters for the reduction of switching losses (SL) and electromagnetic interference (EMI) distortions, especially in dc/dc applications [1]–[5] and also in ac/dc and dc/ac applications [6]–[9]. Although wide band-gap devices such as SiC MOSFETs offer superior switching behavior compared to silicon devices [10]–[14], the soft-switching losses (SSL) of these devices (especially for high blocking voltages in the range of 10 kV) are not negligible. Therefore, it is very important to consider the SSL during the design process. However, most of the device datasheets only provide data for hard-switching losses, which means that it is necessary to experimentally determine the SSL of the particular devices.

Manuscript received February 21, 2017; revised May 16, 2017; accepted July 6, 2017. Date of publication July 20, 2017; date of current version February 22, 2018. Recommended for publication by Associate Editor J. Wang. (*Corresponding author: Daniel Rothmund*.)

The authors are with the Power Electronic Systems Laboratory, ETH Zurich, Zurich 8092, Switzerland (e-mail: rothmund@lem.ee.ethz.ch; bortis@lem.ee.ethz.ch; kolar@lem.ee.ethz.ch).

Color versions of one or more of the figures in this paper are available online at <http://ieeexplore.ieee.org>.

Digital Object Identifier 10.1109/TPEL.2017.2729892

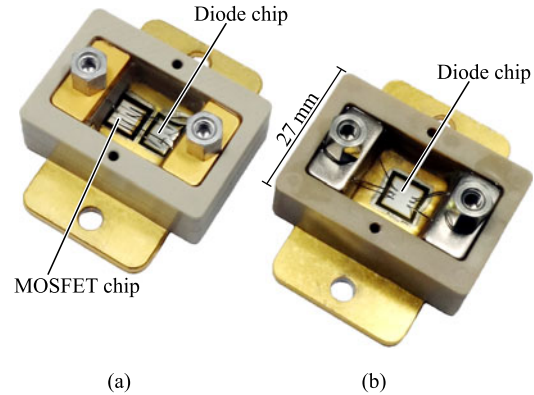


Fig. 1. Pictures of the 10-kV SiC devices: (a) Co-Pack module with a SiC MOSFET chip and an antiparallel SiC junction barrier Schottky (JBS) diode chip, and (b) discrete packaged 10-kV SiC JBS diode.

There are basically two types of SL measurement methods, namely electrical and calorimetric measurement methods. Electrical methods, such as the well-known double pulse test, feature the advantage of a rather short measurement time, since only pulse measurements have to be performed. Furthermore, with the same measurement setup, both the hard-switching losses and the SSL can be directly determined at different chip temperatures by electrically measuring the device voltage and current during a turn-on and a turn-off transient. However, due to the fast switching transients, the accuracy of the measured waveforms strongly decreases, thus the measured SL can be highly inaccurate. In [15], the error analysis for fast switching 10-kV SiC MOSFETs showed that, in the case of SSL measurements, electrical measurement methods, such as the double pulse test, can be subject to measurement errors of more than 200%. Hence, the double pulse method is unsuitable for the measurement of SSL.

In contrast to the electrical measurements, with a calorimetric measurement setup, the semiconductor losses, i.e., the sum of the SL and the conduction losses (CL), are determined by measuring the dissipated power of the device under test (DUT) in continuous operation and, since no fast switching transients have to be measured, typically a higher measurement accuracy is achieved. However, the higher accuracy is reflected in a much longer measurement time due to the large thermal time constants of calorimetric measurement setups. There the total

semiconductor losses can be measured either in the thermal equilibrium or in the transient heat-up phase. For example, in [16], a half-bridge as part of a synchronous buck converter is operated continuously in a double chamber calorimeter until the thermal equilibrium is reached. The SSL of the half-bridge are finally obtained by subtracting the losses of the gate drives, the PCB, and the dc-link capacitor from the total losses measured in the calorimeter. In order to reduce the measurement time of calorimetric measurements, in [17], a transient calorimetric method is presented, whereby a metal block is attached to the switches of a half-bridge circuit that is continuously operated. The metal block acts as a thermal capacitance, which is heated up by the dissipated power of the switches, resulting in a certain temperature increase. Consequently, based on the resulting temperature slope, the dissipated power can be calculated. A further advantage of this method is that, e.g., the gate driver and PCB losses do not have to be subtracted from the measured losses due to the low thermal coupling. Nevertheless, in both the calorimetric measurement methods, the CL (which might be in the same range as the SSL) have to be subtracted from the total measured semiconductor losses, in order to obtain the pure SL. Hence, the accuracy achieved with calorimetric measurements strongly depends on the accurate determination of the CL. In principle, the CL can be calculated based on the DUT's on-state resistance  $R_{DS, on}$  given in the manufacturer's datasheet. However, the  $R_{DS, on}$  of the 10-kV SiC MOSFET examined in this paper [CPM3-10000-0350 from Wolfspeed, cf., Fig. 1(a)] shows a strong dependence on the device current, the chip temperature, and the current direction (approximately above 10 A, the antiparallel JBS diode [CPW3-10000-Z020B from Wolfspeed, cf., Fig. 1(b)] starts conducting), and even deviates from device to device by more than 20%, because the MOSFETs at hand are prototype devices. In order to separate the CL and the SL directly in the measurement, a novel calorimetric SSL measurement method featuring a superior measurement accuracy is proposed in Section II. In Section III-B, this method is applied to the aforementioned 10-kV SiC MOSFETs. The obtained SSL for different dc-link voltages, currents, and gate resistors are presented and can be utilized, e.g., in the design optimization of medium-voltage converters [18]–[20]. Furthermore, even though the measured SSL are small, a deeper analysis concerning the origin of the SSL is performed, since they cannot be explained by the overlapping of the MOSFET voltage and MOSFET current during the switching transients. Therefore, it is assumed that the SSL are arising to a large extent from the charging and discharging of the parasitic output capacitances of the MOSFET and the antiparallel JBS diode, as also stated in [21] and [22]. In Section IV, this assumption is experimentally verified with the proposed measurement method, which on one hand allows to measure the charging/discharging losses (CDL), and on the other hand enables to allocate them to the MOSFET and the JBS diode. Section V finally provides the conclusion and an outlook.

## II. FUNCTIONAL PRINCIPLE OF THE PROPOSED MEASUREMENT METHOD

The basic idea of the proposed method for the measurement of SSL on one hand is to measure the semiconductor losses

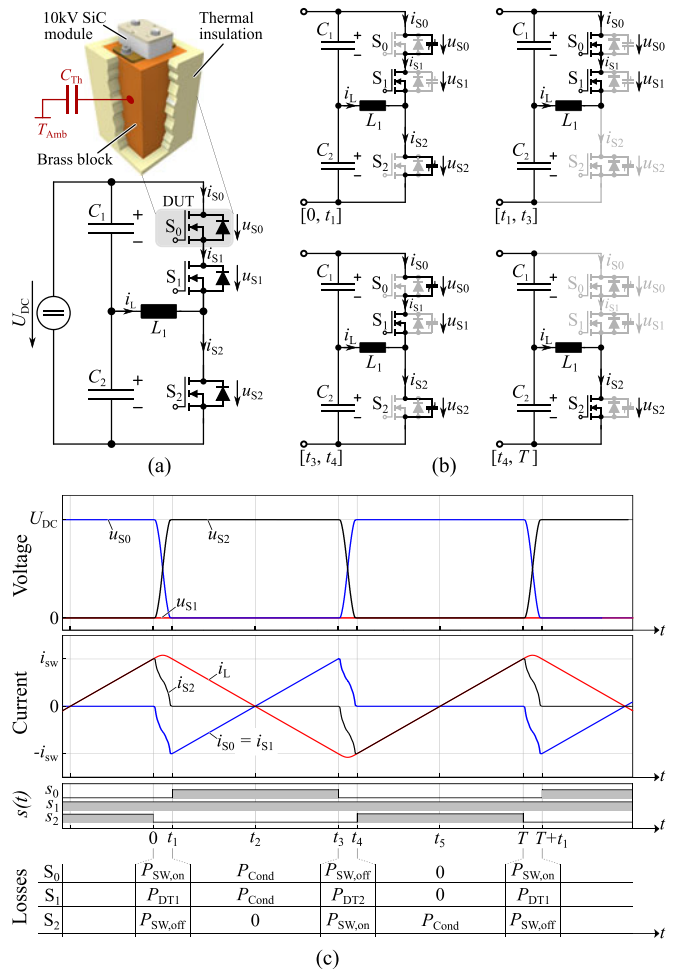


Fig. 2. (a) Circuit diagram with an additional MOSFET  $S_0$  mounted on a thermally insulated brass block, which acts as a thermal capacitance  $C_{Th}$ . (b) Circuit diagrams showing the current path during the specific time intervals; shaded symbols do not conduct current. (c) Ideal current and voltage waveforms as well as the gate signals of the three switches and the corresponding share of losses in each time interval.

calorimetrically and on the other hand to measure the SL and the CL separately. Therefore, as shown in Fig. 2(a), a third MOSFET  $S_0$  is inserted in series either to the low-side switch  $S_2$  or the high-side switch  $S_1$  of the half-bridge. In the following, it is assumed that  $S_0$  is connected in series to the high-side switch  $S_1$  since the cooling pad of the DUT is connected to the drain potential of the MOSFET and thus in this configuration is fixed to a stable voltage. Furthermore, the MOSFET module  $S_0$  is mounted on top of a brass block, which absorbs the dissipated semiconductor losses and acts as a thermal capacitance  $C_{Th}$  [cf., Fig. 2(a)]. Brass is selected as heat sink material due to its high thermal capacitance per volume. In addition, the brass block is isolated with thermal insulation material in order to minimize the heat transfer to the ambient. Consequently, assuming a constant power dissipation in the semiconductor device  $S_0$ , the temperature of the brass block linearly increases over time, whereby the temperature slope is proportional to the dissipated power of  $S_0$ . Hence, the power dissipation of  $S_0$  can be calculated as

$$P = \frac{C_{Th} \cdot \Delta\vartheta}{\Delta\tau} \quad (1)$$

where  $\Delta\vartheta$  denotes the temperature difference and  $\Delta\tau$  equals the measurement time. Based on (1), the dissipated power of  $S_0$  can now be determined by operating the half-bridge continuously, and by measuring the time  $\Delta\tau$ , which is required to heat the insulated brass block by a certain temperature difference  $\Delta\vartheta$ , e.g., from 30 °C to 40 °C.

For the basic operation of the modified half-bridge shown in Fig. 2(a), the series connection of  $S_0$  and  $S_1$  can be considered as one switch, where either  $S_0$  or  $S_1$  is permanently turned ON, whereas the other is complementarily switched with  $S_2$ , i.e., the circuit behaves like a conventional half-bridge. Hence, in order to achieve soft-switching transitions in all switches, the half-bridge is continuously operated with a 50% duty cycle resulting in a triangular current, as shown in Fig. 2(c). As can be noticed, the shown section corresponds to a moment in time in which  $S_1$  is permanently turned ON, whereas  $S_0$  and  $S_2$  are complementarily switching. Consequently, due to the series connection of  $S_0$  and  $S_1$ , the same current is flowing through both switches, which means that the CL in both switches are the same if equal on-state resistances  $R_{DS,ON}$  are assumed. Furthermore, since only  $S_0$  and  $S_2$  are switching, the SSL are only generated in  $S_0$  and  $S_2$ , whereas  $S_1$  only generates CL. Accordingly, if one would separately measure the losses in both MOSFETs  $S_0$  and  $S_1$  based on (1), the SSL generated in  $S_0$  could be directly extracted from the loss difference in the two semiconductor devices.

However, since the on-state resistance  $R_{DS,ON}$  is strongly varying from device to device in this case, as already mentioned, the SL and the CL cannot be properly separated from each other. Therefore, instead of measuring the losses of two different devices  $S_0$  and  $S_1$  at the same time, in addition to the measurement  $M_1$  discussed above, a second measurement  $M_2$  is performed at the same operating conditions, i.e., the same switched current, dc-link voltage, dead time, switching frequency, and temperature range. In measurement  $M_2$ , however, the MOSFETs  $S_0$  and  $S_1$  swap their roles such that  $S_0$  is now permanently ON and  $S_1$  is complementarily switched with  $S_2$ . In this case,  $S_0$  only generates CL ( $P_{M2} = P_{Cond}$ ), while during measurement  $M_1$  the MOSFET  $S_0$  was generating both, SL and CL, i.e., ( $P_{M1} = P_{Cond} + P_{SW}$ ). Hence, the SSL of  $S_0$  within one switching period can be found by subtracting  $P_{M2}$  from  $P_{M1}$  and dividing the difference by the switching frequency.

Unfortunately, even though in both measurements  $M_1$  and  $M_2$  the CL are measured in the same device for the same operating conditions, the CL are not exactly identical due to the dead time intervals  $[0, t_1]$  and  $[t_3, t_4]$ , where the output capacitances of the switches have to be charged/discharged. In order to emphasize the importance of the dead time intervals in the calculation of the CL, in Fig. 2(c) the switched current is chosen rather small, which means that the dead time intervals can occupy a significant part of a switching period. It should be noted that the length of the dead time intervals  $[0, t_1]$  and  $[t_3, t_4]$  is selected in such a way that the corresponding switch is turned ON exactly at the moment when its drain-source voltage reaches 0 V, i.e., ideally the antiparallel JBS diodes are not conducting. Actually, since  $S_1$  is connected in series to  $S_0$ , in the first measurement  $M_1$  the MOSFET  $S_1$  should only generate CL during the on-state interval

of  $S_0$ . However, as shown in Fig. 2(b), during the dead time intervals  $[0, t_1]$  and  $[t_3, t_4]$ , the current, which flows through the nonlinear output capacitance of  $S_0$ , also flows through the MOSFET channel of  $S_1$ , generating additional CL  $P_{DT1}$  and  $P_{DT2}$  in  $S_1$  ( $P_{DT} = P_{DT1} + P_{DT2}$ ). Consequently, during the second measurement  $M_2$  ( $S_0$  permanently on,  $S_1$  switching), the same additional CL  $P_{DT}$  arise in  $S_0$  and thus have to be considered for the calculation of the SSL. As described in [15], the CL  $P_{DT}$ , which occur during the dead time, can be calculated as

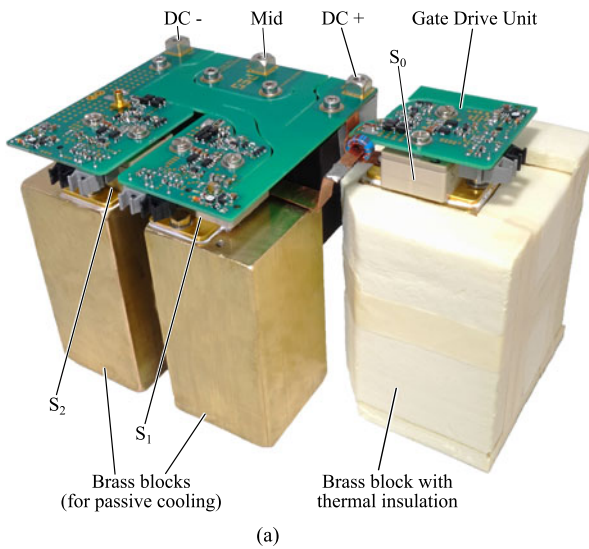
$$P_{DT} = h_P \cdot P_{Cond}, \text{ where} \quad (2)$$

$$h_P = \frac{R_{DS,ON} \cdot \int_0^{t_1} i_{S0}^2 \cdot dt}{R_{DS,ON} \cdot \int_{t_1}^{t_2} i_{S0}^2 \cdot dt} \approx \frac{\int_0^{t_1} i_{S0}^2 \cdot dt}{\int_{t_1}^{t_2} i_{S0}^2 \cdot dt}. \quad (3)$$

Thereby,  $h_P$  can be obtained by measuring the drain current of  $S_0$  and by solving the given integrals for the corresponding time intervals.

As will be discussed in Section III-A, in order to achieve a high measurement accuracy, the SSL should account for the largest share of the overall power dissipation measured at the brass block, since in this case, the sensitivity of the SSL on calculation errors of  $h_P$  as well as on variations in the CL between the two measurements, e.g., due to the temperature-dependent  $R_{DS,ON}$  of  $S_0$ , is very low. Accordingly, for the dimensioning of the brass block, it is assumed that in the worst case, i.e., max. switched current of 15 A, the CL should not exceed 50% of the SSL, which in contrast to the CL can be adapted via the switching frequency and the inductance value. The  $R_{DS,ON}$  of the 10-kV SiC MOSFETs at hand is around 0.35 Ω at room temperature, which in the worst case results in 13 W of CL, and according to this rule in a total power dissipation of 39 W. Furthermore, in order to achieve a minimum relative accuracy of ±1% for the temperature measurement, the measurement range must be at least  $\Delta\vartheta = 10$  K, if an absolute temperature measurement error of ±0.1 K is expected. For the same reason of measurement accuracy, the minimum measurement time  $\Delta\tau$  should be at least 2–3 min. Hence, the required thermal capacitance and therewith the size of the brass block (50 mm × 50 mm × 100 mm) can be calculated based on (1). A picture of the corresponding 10-kV SiC hardware setup with the thermally insulated brass block is shown in Fig. 3(a). It should be noted that the MOSFETs  $S_1$  and  $S_2$  are also mounted on separate brass blocks instead of heat sinks in order to not distort the measured temperature of the insulated brass block by any air stream.

In order to obtain the precise thermal capacitance of the brass block in the hardware setup, the value  $C_{Th}$  has to be calibrated by measurements. Therefore, a constant dc-power is fed into the MOSFET module by driving a feedback-controlled current through the device such that the constant power levels of 10, 20, 40, and 60 W are reached. Thereby, the hardware configuration (including the copper busbars to the dc-link, the gate drive, and the thermal insulation, etc.) must be exactly the same as it is later used for the SSL measurements. Figs. 3(b)–(e) show the measured temperature profiles of the insulated brass block for the different power ratings. It can be seen that between 30 °C and 40 °C the measurements for 20 and 40 W are completely linear, whereas for 10 and 60 W certain nonlinearities are measured



(a)

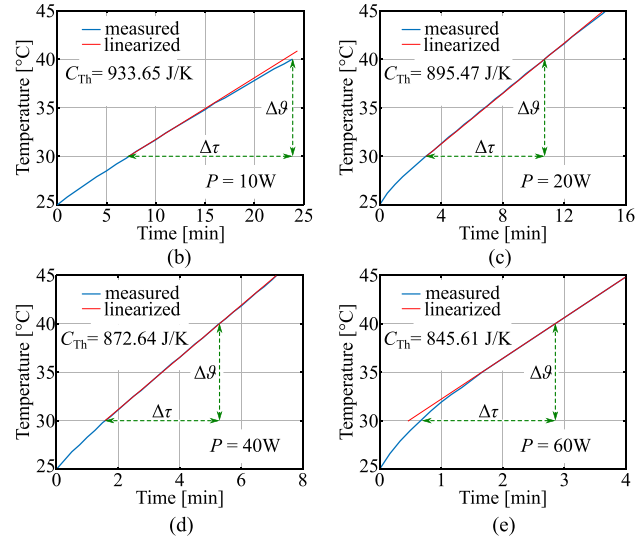


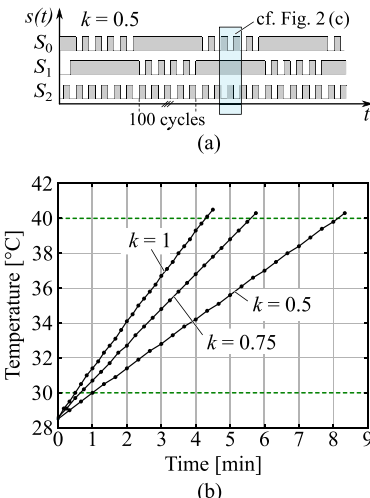
Fig. 3. (a) 10-kV SiC half-bridge with the additional MOSFET  $S_0$  on a thermally insulated brass block ( $50 \text{ mm} \times 50 \text{ mm} \times 100 \text{ mm}$ ). (b)–(e) Thermal calibration measurements at constant dc power levels, (b) 10 W, (c) 20 W, (d) 40 W, and (e) 60 W. Each temperature profile is linearized around the measurement temperature range and the corresponding thermal capacitance is calculated for the given slope. A high linearity can be achieved in the temperature range from  $30^\circ\text{C}$  to  $40^\circ\text{C}$  and the power range from 20 to 40 W. Thus, all the SL measurements are carried out in this power and temperature range.

in the temperature curves. Consequently, all SSL measurements are performed in the power range from 20 to 40 W and in the temperature range from  $30^\circ\text{C}$  to  $40^\circ\text{C}$ . Furthermore, as indicated in Figs. 3(b)–(e), the linearized thermal capacitance  $C_{\text{Th}}$  is slightly changing within the selected power range. Therefore,  $C_{\text{Th}}$  is interpolated iteratively from the calibration measurements for the purpose of obtaining the correct power dissipation.

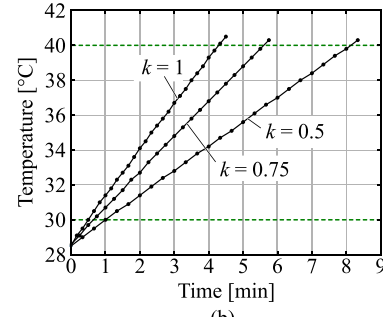
Due to this limitation in the power range, now the problem of measuring only CL in measurement  $M_2$  arises, since for small switched currents the CL are in the range of only 1–2 W. In order to overcome this problem, the operation principle of the half-bridge has to be modified in such a way that also in the measurement  $M_2$  higher losses are generated in  $S_0$ . Therefore, instead of permanently turning on  $S_0$ ,  $S_0$  and  $S_1$  share the switching actions and therewith the SL among each other, as indicated in Fig. 4(a). The share of the switching cycles, which is switched by  $S_0$ , is defined as the switching cycle share  $k$ . A value of  $k = 1$  means that  $S_0$  is switching continuously, whereas  $S_1$  is permanently turned ON. As an example, in Fig. 4(a),  $k$  is equal to 0.5, which means that  $S_0$  and  $S_1$  are alternatingly switching 50% of the total switching cycles and are constantly turned ON for the other 50%. For practical reasons,  $S_0$  and  $S_1$  are alternated for every 100 switching cycles. In Fig. 4(b), measured temperature profiles at  $U_{\text{DC}} = 8 \text{ kV}$  and a switched current of 7.5 A are shown for different values of  $k$ . As can be noticed, the measurements follow a linear characteristic, which means that the thermal setup is operated in its linear region as desired.

Accordingly, depending on the selected switching cycle share  $k$ , the average losses  $P_{S0}$  of  $S_0$  within one measurement can be brought into the optimum power range of 20 to 40 W and can be expressed in general terms as

$$\begin{aligned} P_{S0} &= k(P_{\text{SW}} + P_{\text{Cond}}) + (1 - k)(P_{\text{DT}} + P_{\text{Cond}}) \\ &= k \cdot P_{\text{SW}} + P_{\text{Cond}} + (1 - k)P_{\text{DT}} \end{aligned} \quad (4)$$



(a)



(b)

Fig. 4. (a) Gate signals of the three MOSFETs for the modified modulation scheme exemplarily shown for a switching cycle share of  $k = 0.5$ . (b) Measured temperature curves for  $U_{\text{DC}} = 8 \text{ kV}$ ,  $i_{\text{Switched}} = 7.5 \text{ A}$  and different values of  $k$ .

where  $P_{\text{SW}} = P_{\text{SW},\text{on}} + P_{\text{SW},\text{off}}$  and  $P_{\text{DT}} = P_{\text{DT},1} + P_{\text{DT},2}$ . Hence, in the first measurement  $M_1$  where  $k = 1$ , the power dissipated in  $S_0$  is

$$P_{M1} = P_{S0} (k = 1) = P_{\text{SW}} + P_{\text{Cond}}. \quad (5)$$

In the second measurement  $M_2$  where  $k < 1$ , the dissipated power in  $S_0$  is given as

$$P_{M2} = k \cdot P_{M1} + (1 - k)(P_{\text{Cond}} + P_{\text{DT}}) \quad (6)$$

where  $P_{\text{SW}} = P_{M1} - P_{\text{Cond}}$  from (5) is used. Furthermore, based on (2), the dead time losses  $P_{\text{DT}}$  in (6) can be substituted by  $h_P \cdot P_{\text{Cond}}$ ; thus, the effective CL and SL are given

as

$$P_{\text{Cond}} = \frac{P_{M2} - k \cdot P_{M1}}{1 - k + (1 - k) \cdot h_P}, \quad (7)$$

$$P_{\text{SW}} = P_{M1} - P_{\text{Cond}} \quad (8)$$

and they only depend on the two measured losses  $P_{M1}$  and  $P_{M2}$  as well as on the selected switching cycle share  $k$ . For the SSL measurements of the 10-kV SiC MOSFETs, a switching cycle share of  $k = 1$  has been chosen for measurement  $M_1$ ,  $k = 0.5$  for measurement  $M_2$  and  $k = 0.75$  for a third (verification) measurement, leading to stable and reproducible results. Finally, the SL per MOSFET and switching period can be determined as  $E_{\text{SW}} = P_{\text{SW}} / f_{\text{SW}}$ .

### III. DISCUSSION AND EXPERIMENTAL RESULTS

The following section analyzes the accuracy of the proposed SSL measurement method and discusses possible limitations and sources of measurement errors. Finally, the measured SSL are presented and discussed.

#### A. Error Analysis for the Proposed SSL Measurement Method

Although calorimetric measurements are probably the most direct and accurate way of measuring power dissipations, there are several effects that need to be considered in order to obtain accurate results. First, an accurate and EMI robust measurement of the brass block temperature is required. Depending on the device package, the cooling terminal might be on drain potential of the MOSFET (which is the case for the 10-kV SiC MOSFETs at hand) such that the metal block including the temperature sensor is on (floating) potential and is possibly exposed to high  $dU/dt$  values, which could disturb the temperature measurement. Furthermore, the position of the temperature sensor on the metal block must be the same during the calibration and the SL measurements. Otherwise, measurement errors could arise due to a possibly inhomogeneous temperature distribution within the metal block. In the given setup, a thermocouple was attached to the top side of the brass block, next to the baseplate of the 10-kV SiC module. A better approach would be to use a fiber optic temperature sensor, which besides the EMI robustness also provides a galvanic isolation. Generally important for this measurement method is the thermal decoupling of the DUT and its brass block from the ambient (by applying thermal insulation material to the brass block) and especially from other heat sources contained in the hardware setup (such as the other switches) in order to prevent undesired heat transfers to the brass block. This is easily possible for the 10-kV SiC MOSFETs at hand due to the specific package design and the anyway required distances between the switch and other parts of the circuit for the reason of electrical isolation. The measured thermal time constant of the thermally insulated brass block together with the 10-kV SiC module is  $\tau_{\text{Block}} = 200$  min, which is a factor of 15 larger than the maximum measurement time. This shows that the undesired heat transfers to the ambient and other parts of the setup can be neglected in the given setup. For other device packages and especially lower voltage devices, however, the thermal decoupling of the DUT might be

TABLE I  
MEASURED AND CALCULATED VALUES FOR THE CASE OF LOW SWITCHED CURRENT (7 kV, 2.5 A) AND HIGH SWITCHED CURRENT (7 kV, 15 A)

Parameter	Value for 7 kV, 2.5 A	Value for 7 kV, 15 A
$P_{M1}$	37.50 W	38.54 W
$P_{M2}$	18.84 W	26.99 W
$h_P$	1.1883	0.0731
$P_{\text{Cond}}$	0.09 W	14.38 W
$P_{\text{SW}}$	37.41 W	24.16 W
$P_{\text{DT}}$	0.10 W	1.05 W
$f_{\text{SW}}$	200 kHz	100 kHz

a problem, since a thermal decoupling goes hand in hand with an increase of the commutation loop inductance, which could lead to voltage overshoots and ringing. For the employed 10-kV devices operated with dc-link voltages in the kilovolt range, the voltage overshoot caused by the additional inductance of the third switch is negligible and not even measurable.

Since the measurement method includes a measurement of a rather small temperature difference  $\Delta\vartheta$  of 10 K, the accuracy of the temperature measurement is the most critical parameter. Assuming a measurement error of  $\Delta\vartheta = \pm 0.1$  K (which corresponds to a relative error of  $\pm 1\%$ ), a  $\pm 2\%$  error in the thermal capacitance  $C_{\text{Th}}$  and a perfect time measurement (since time can be measured very precisely), the worst case error of a single power measurement is  $\pm 3\%$  (cf., (1),  $102\% \cdot 101\% \approx 103\%$ ). Hence, as a worst case estimation, if  $P_{M1}$  is measured 3% too high and  $P_{M2}$  is measured 3% too low, the relative errors in the SL are 5.8% for the 7 kV, 2.5 A case and 15.5% for the 7 kV, 15 A case, whereby measured values for  $P_{M1}$ ,  $P_{M2}$ , and  $h_P$  (cf., Table I) are inserted into (7) and (8) for the error analysis in order to give practical examples. Compared to the double pulse method, a 10 to 20 times higher accuracy can be achieved with the proposed calorimetric method [15]. Furthermore, in all the performed measurements, the  $k = 0.5$  and the  $k = 0.75$  (reference) measurements match within 5% error, which demonstrates that the worst case is not very likely to occur if the measurements are carried out carefully and indicates that the accuracy of the method is very high. As can be noticed, the measurement error increases with increasing switched currents, thus the SL should hold the largest share of the overall measured power dissipation in order to keep the measurement accuracy high. This can be managed by choosing a rather high switching frequency, which however is limited by certain constraints such as the gate drive power capability, the total generated losses on the metal block (which might be too high and result in a nonlinear temperature profile at some point) or the fact that with higher switching frequencies the dead time interval consumes a major part of the overall switching cycle. Another (limited) possibility to increase the measurement accuracy is to increase the temperature difference  $\Delta\vartheta$ . However, the temperature dependence of the MOSFET properties might start playing a role for higher values of  $\Delta\vartheta$ . For example, in the derivation of the SL from the two measurements  $M_1$  and  $M_2$ , in (3) it is assumed that the on-state resistance  $R_{\text{DS},\text{on}}$  is constant, however, this is not true, because the  $R_{\text{DS},\text{on}}$  of the 10-kV SiC MOSFETs at hand

depends on the temperature as well as on the direction and the value of the drain current. Hence, the  $R_{DS,on}$  does not completely cancel out in (3) and leads to a certain calculation error of  $h_P$ . However, the sensitivity of the SSL on calculation errors of  $h_P$  is very low. On one hand, for low switched currents, the switching frequency is selected rather high (cf., Table I) in order to increase the SL until an optimal power dissipation between 20 and 40 W on the brass block is achieved. In this case, the dead time indeed consumes a major part of the switching cycle ( $h_P \approx 1$ ), thus the corresponding losses  $P_{DT}$  are similar to the CL  $P_{Cond}$  (cf., Table I). Due to the low current rating, however, the SL  $P_{SW}$  are orders of magnitude higher than  $P_{DT}$  or  $P_{Cond}$ . Consequently, calculation errors of  $h_P$  hardly influence the SL, e.g., with the values given for the 7 kV, 2.5 A measurement in Table I, the SL error stays below 0.012%, if for the determination of  $h_P$  a calculation error of  $\pm 10\%$  is assumed. On the other hand, for high switched currents, the time to charge/discharge the output capacitances of the MOSFETs is short, i.e.,  $h_P \approx 0$ . Hence, errors in the calculation of  $h_P$  have a negligible impact on the SL. Assuming again an error of  $\pm 10\%$  in  $h_P$ , for the case of 7 kV, 15 A (cf., Table I), the SL error is below 0.41%.

Furthermore, a measurement error could potentially result due to the fact that the chip temperature and therewith the  $R_{DS,on}$  are not equal in the two measurements  $M_1$  and  $M_2$  since the generated losses  $P_{M1}$  and  $P_{M2}$  are different, which results in distinct junction temperatures. Therefore, the impact of this junction temperature difference on the measuring accuracy is analyzed in the following. As stated above, the influence of the dead time can be neglected ( $P_{DT} \approx 0$ ), thus with the simplified equations (5) and (6) and the assumption of equal average CL  $P_{Cond}$  within the two measurements, the SL  $P_{SW}$  can be immediately expressed by the difference of the two measured losses  $P_{M1}$  and  $P_{M2}$  as

$$\Delta P_{M12,ideal} = P_{M1} - P_{M2} = P_{SW} (1 - k). \quad (9)$$

Due to this difference in losses, however, the thermal resistance between the chip and the brass block  $R_{JB}$  leads to a higher junction temperature in measurement  $M_1$  compared to  $M_2$ , even though both measurements are performed for the same brass block temperature range from 30 °C to 40 °C. Assuming a thermal resistance of  $R_{JB} = 0.5 \text{ KW}^{-1}$  (extracted from thermal FEM simulations) and exemplarily measured losses of  $P_{M1} = 30 \text{ W}$  and  $P_{M2} = 20 \text{ W}$ , the chip temperature in  $M_1$  would (ideally) pass through the temperature range of  $30 \text{ }^{\circ}\text{C} + R_{JB} \cdot P_{M1} - 40 \text{ }^{\circ}\text{C} + R_{JB} \cdot P_{M1} = 45 \text{ }^{\circ}\text{C} - 55 \text{ }^{\circ}\text{C}$ , whereby the chip temperature in  $M_2$  passes through the temperature range of  $40 \text{ }^{\circ}\text{C} - 50 \text{ }^{\circ}\text{C}$ , i.e., there is an average chip temperature difference of 5 K. Consequently, since the on-state resistance  $R_{DS,on}$  of the employed 10-kV SiC MOSFETs features a temperature dependence of  $\Delta R = 1\% \text{K}^{-1}$ ; in this example, the actual average CL in  $M_1$  are 5% higher than in  $M_2$ . Hence, considering a linear increase of the  $R_{DS,on}$  with temperature, (5) and (6) have to be adapted to

$$P_{M1} = P_{SW} + (1 + \beta) \alpha P_{SW} \quad (10)$$

$$P_{M2} = k \cdot P_{SW} + \alpha P_{SW} \quad (11)$$

with

$$\alpha = \frac{P_{Cond}}{P_{SW}} \quad \text{and} \quad (12)$$

$$\beta = R_{JB} \cdot \Delta P_{M12,ideal} \cdot \Delta R \quad (13)$$

where  $\alpha$  is the ratio between the CL and the SL (which should always be kept as small as possible by properly choosing the switching frequency) and  $\beta$  is the relative increase of the MOSFET's  $R_{DS,on}$  depending on the loss difference between the two measurements  $M_1$  and  $M_2$ . Subtracting (10) from (11) leads to

$$\begin{aligned} \Delta P_{M12,real} &= (1 - k + \alpha\beta) P_{SW} \\ &= \Delta P_{M12,ideal} \left( 1 + \frac{\alpha\beta}{1 - k} \right). \end{aligned} \quad (14)$$

Now, the relative error  $e_{\Delta T}$  introduced by the junction temperature difference between  $P_{M1}$  and  $P_{M2}$  can be found as

$$e_{\Delta T} = \frac{\alpha\beta}{1 - k}. \quad (15)$$

It should be noted that this analysis is also valid for devices with a nonlinear dependence of the  $R_{DS,on}$  on temperature, since in this case, the  $R_{DS,on}$  can be linearized within the relevant temperature range of 10 K from, e.g., 45 °C to 55 °C with a high accuracy. For the values given in Table I, (15) leads to a relative error  $e_{\Delta T}$  in the range of 0.05%–6.87%, which means that the worst case error for the measurements following in Section III-B is smaller than 7%. As can be noticed, the error increases with increasing current, since the ratio  $\alpha$  between the CL and the SL increases. In order to keep the error small, the objective should be to achieve  $\alpha \leq 1$  (which means  $P_{M1} - P_{M2} \leq 20 \text{ W}$  for the setup at hand). Nevertheless, if the exact values of  $R_{JB}$  and  $\Delta R$  of the MOSFET are known, this error can be corrected in the loss calculation. Finally, it should be noted that the SSL do not or hardly depend on the junction temperature, as will be shown later.

## B. Measurement Results

In order to cover a wide range of applications in which the analyzed 10-kV SiC MOSFETs could be utilized, SSL measurements have been performed for different dc-link voltages, currents, and gate resistors. Fig. 5 shows the net measured SSL of the 10-kV SiC MOSFETs for dc-link voltages between 4 and 8 kV and switched currents between 2.5 and 15 A. Unless otherwise noted, the gate resistors are  $R_{on} = 20 \Omega$  and  $R_{off} = 10 \Omega$ . It is clearly visible that the SSL depend mainly on the dc-link voltage and increase only slightly with increasing current. This behavior will be discussed in more detail in Section IV. Compared to the hard-switching operation of these 10-kV SiC MOSFETs, cf., [23], almost a factor 100 lower SL can be achieved by applying soft-switching techniques, which enables higher switching frequencies, efficiencies, and power densities. Comparing the three 7-kV curves with different turn-off gate resistors  $R_{off}$  in Fig. 5, it is evident that a turn-off resistor of  $R_{off} = 10 \Omega$  leads to the lowest SSL. For the case of  $R_{off} = 15 \Omega$ , the dependence on the switched current shows a clear trend toward higher losses for higher switched currents, which is an indication for

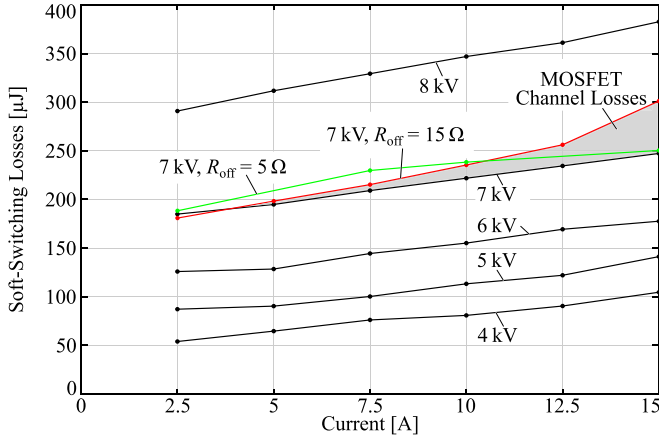


Fig. 5. Calorimetrically measured SSL of the 10-kV SiC MOSFETs for different dc-link voltages, switched currents, gate resistors, and a measurement temperature range of 30 °C–40 °C. Unless otherwise noted, the turn-off gate resistor is  $R_{\text{off}} = 10 \Omega$ .

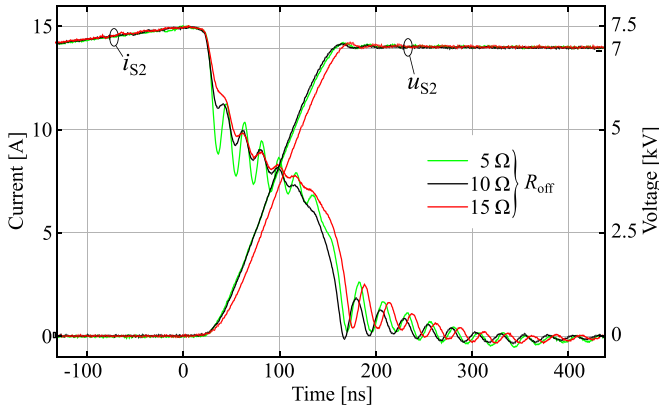


Fig. 6. Comparison of soft-switching transitions for different turn-off gate resistors at  $U_{\text{DC}} = 7 \text{ kV}$  and  $i_{\text{Switched}} = 15 \text{ A}$ .

increased channel losses due to a larger overlapping of the voltage and current transients during turn-off. This behavior can be explained by analyzing the soft-switching transitions given in Fig. 6 for 7 kV and 15 A. While the switching transitions are almost equally fast for turn-off gate resistors of 5 and 10 Ω, the switching transition for a gate resistor of 15 Ω is clearly slowed down. Hence, especially for higher switched currents, the higher gate resistor leads to a stronger overlapping of the MOSFET voltage and channel current transients and thus to higher SL. On the other hand, a low turn-off gate resistance of 5 Ω results in stronger oscillations in the drain current due to parasitic inductances introduced by the semiconductor packaging and thus causes higher SSL. Consequently, for the 10-kV SiC MOSFETs at hand, the optimum turn-off gate resistance is  $R_{\text{off}} = 10 \Omega$ , which could be probably slightly decreased if another package with lower parasitic inductances and/or with Kelvin source connection is used. However, even though the packaging can be improved, a substantial reduction of the SSL is not expected. Furthermore, it should be mentioned that the turn-on resistor does not or hardly influence the SSL.

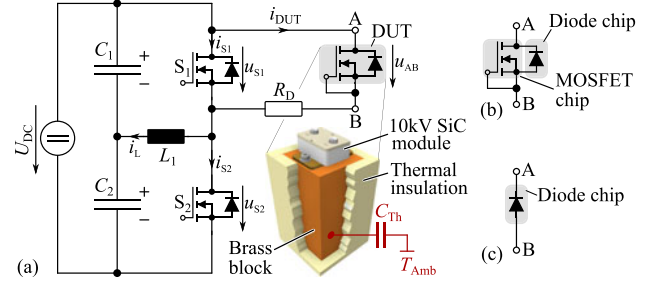


Fig. 7. (a) Circuit diagram of the CDL measurement setup. The DUT (permanently turned OFF) is connected in parallel to the high-side switch via a damping resistor  $R_D$ . The two possible DUTs: (b) Co-Pack module consisting of a SiC-MOSFET chip and an antiparallel JBS diode chip and (c) discrete packaged JBS diode.

#### IV. OUTPUT CAPACITANCE CHARGING/DISCHARGING LOSSES (CDL)

In Fig. 5, it is clearly visible that the measured SSL are strongly dependent on the dc-link voltage (with an approximately quadratic relation  $E_{\text{SW}} \sim U_{\text{DC}}^2$ ) whereas the dependence on the switched current is linear with a rather flat and voltage-independent slope. Furthermore, the SSL curves do not pass through the origin, if they are extrapolated toward zero current. In contrast, the curves show a voltage-dependent offset, which means that there are voltage-dependent residual SSL, which cannot be avoided. This indicates that a large share of the SSL might just arise from the charging and discharging of the parasitic output capacitances of the MOSFET and the antiparallel JBS diode, and only a minor share of the SSL is caused by the overlap of the MOSFET's voltage and channel-current transients. The loss mechanisms related to the charging/discharging of the nonlinear output capacitance have already been discussed for superjunction MOSFETs [22], [24], where significant fractions (strongly depending on the device) of the stored energy in the output capacitance are lost during the charging/discharging process. (In [25], this effect is explained via a mixed-mode simulation of low-voltage superjunction MOSFETs). In the following, an accurate calorimetric method to measure the CDL is presented. Furthermore, in order to identify to which component the CDL have to be allocated, i.e., the MOSFET or the antiparallel JBS diode, on one hand the proposed method is applied to a module consisting of a 10-kV SiC MOSFET with an antiparallel JBS diode [cf., Fig. 1(a)], and on the other hand to a module containing only a JBS diode [cf., Fig. 1(b)].

##### A. Description of the CDL Measurement Method

For the measurement of the CDL of the 10-kV SiC devices, the same measurement setup as for the determination of the SSL can be used. The DUT is still mounted on a thermally insulated brass block; however, instead of placing the DUT in series, it is now connected in parallel to the high-side switch [cf., Fig. 7(a)], which means that the voltage across the high-side switch is also applied to the DUT. Since only the CDL should be measured, the DUT is permanently kept off by shorting the DUT's gate to the source terminal, thus the DUT only behaves like an additional nonlinear capacitor connected in parallel to the high-side switch.

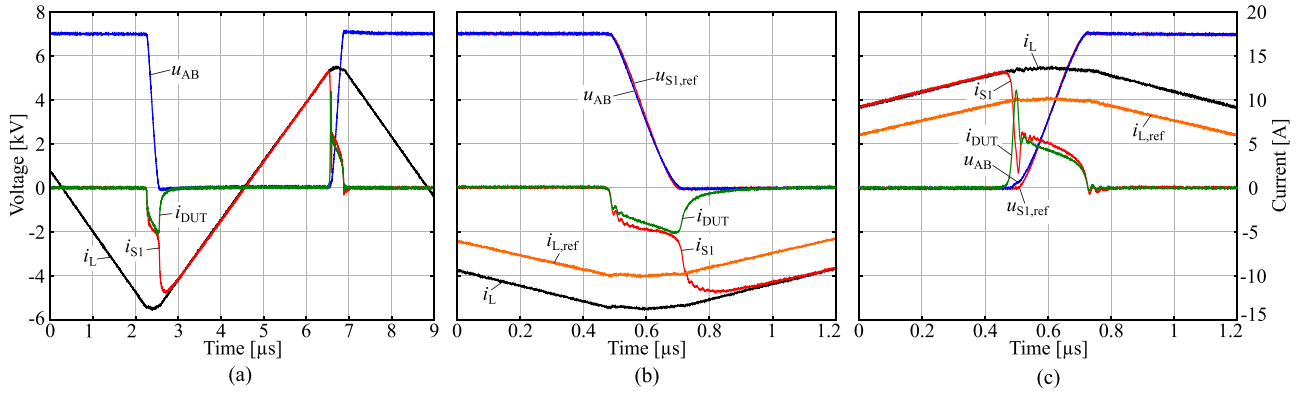


Fig. 8. (a) Current and voltage waveforms of the 7 kV, 10 A-equivalent CDL measurement. Detailed view of the waveforms (b) during the falling voltage transition and (c) during the rising voltage transition, where  $u_{AB}$  is matched to the voltage slope of  $u_{S1,ref}$ , which was obtained from the 7 kV, 10 A SSL measurement.

Due to the parasitic inductances of the module packages and the interconnections, a damping resistor  $R_D$  is added in series to the DUT, in order to avoid any ringing between the DUT and the high-side MOSFET during the switching transitions. In addition, during the on-state of  $S_1$ ,  $R_D$  also prevents the DUT from reverse conduction, i.e., either through the body-diode of the SiC-MOSFET or the antiparallel JBS diode. As shown in Fig. 8(a), there is only a current  $i_{DUT}$  flowing through the DUT during the switching transitions, whereas during the conduction intervals of  $S_1$  and  $S_2$  the current  $i_{DUT}$  is zero.

The value of  $R_D$  was experimentally determined and is set to  $R_D = 20 \Omega$ . It should be noted that, due to the device's relatively high blocking voltage compared to its current rating, the voltage drop across  $R_D$  during the switching transition is negligible compared to the switched voltage, i.e.,  $u_{AB} \approx u_{S1}$ . Hence, the voltage  $u_{AB}$  across the DUT closely follows the high-side MOSFET's voltage  $u_{S1}$  and the output capacitance of the DUT is entirely charged and discharged in each switching cycle. Accordingly, even though the voltage across  $R_D$  is comparatively small, depending on the switching frequency, a significant amount of losses is dissipated in  $R_D$ . Therefore,  $R_D$  has to be thermally decoupled from the DUT in order not to influence the temperature measurement on the DUT's metal block.

Due to the parallel connection of the DUT to the high-side switch, the effective output capacitance of the half-bridge is increased, which means that compared to the SSL measurements for a given switched current the corresponding voltage slope, i.e., the  $du/dt$ , is slowed down. In other words, for a given current, in this setup, the charging current flowing through the DUT is lower compared to the current flowing through the MOSFET's parasitic output capacitance in the SSL measurements. However, in order to be able to properly assign the CDL to the correct SSL measurements, the DUT has to be tested under the same conditions. In this case, this means that the total switched current, i.e., the inductor current  $i_L$ , has to be increased in such a way that in both, the CDL measurement and the SSL measurement, the same  $du/dt$  is achieved. Consequently, based on  $i = C \cdot du/dt$ , also the charging current in the DUT has

to be the same. Exemplarily, Fig. 8(b) and (c) show the measured waveforms during the two switching transients of the CDL measurement, which actually correspond to the SSL measurement carried out at  $i_{L,ref} = 10$  A. As can be noticed, in order to match the voltage slope  $u_{AB}$  to the corresponding voltage slope  $u_{S1,ref}$ , the inductor current  $i_L$  has to be increased to 13.5 A. This ratio between the reference current  $i_{L,ref}$  and the required current  $i_L$  slightly changes with the dc-link voltage and the current level due to the strong nonlinearity of the devices' output capacitances. However, as can be noticed, there is still a small deviation between  $u_{AB}$  and the reference voltage  $u_{S1,ref}$ , which in consequence also leads to a slightly different charging current waveform. The reason is that, due to the parallel connection of the DUT and the high-side switch, the effective output capacitance of the high-side switch is larger than the one of the low-side switch and therefore the half-bridge is no longer symmetrical. This asymmetry can be compensated by also adding a DUT to the low-side switch; however, in this case the total output capacitance of the half-bridge is doubled. Consequently, for the SSL measurement at  $i_{L,ref} = 15$  A (cf., Fig. 5) the corresponding CDL measurement would have to be performed at  $i_L = 30$  A, which is not possible with the given setup. Nevertheless, regardless whether one or two DUTs are used, the current pulses through the DUT are not equal for both transitions [cf., Fig. 8(b) and (c)], since due to the nonlinear output capacitances of the devices, the inductor current  $i_L$  is not equally divided into the high- and low-side switches during the switching transitions. Fig. 9 shows the measured input ( $C_{iss}$ ), reverse transfer ( $C_{rss}$ ), and output capacitance ( $C_{OSS,Co-Pack}$ ) of the Co-Pack, as well as the measured output capacitance of the discrete JBS diode module ( $C_{Diode}$ ) as a function of the applied bias voltage. Furthermore, the output capacitance of the MOSFET chip ( $C_{OSS,MOSFET}$ ), which has been obtained by taking the difference  $C_{OSS,Co-Pack} - C_{Diode}$ , is shown. It can be seen that the output capacitances of the MOSFET and the JBS diode are strongly nonlinear in the lower voltage range. Furthermore, it is evident that for higher voltages, the capacitance of the JBS diode is twice as high as the output capacitance of the MOSFET chip.

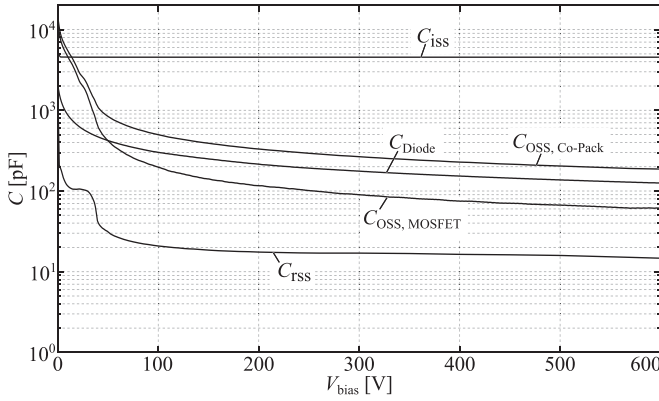


Fig. 9. Measured capacitances of the 10-kV SiC devices as function of the applied bias voltage  $V_{\text{bias}}$ . Note that the output capacitance of the MOSFET chip ( $C_{\text{OSS, MOSFET}}$ ) is obtained by subtracting the measured output capacitance of the Co-Pack ( $C_{\text{OSS, Co-Pack}}$ ) and the output capacitance of the JBS diode ( $C_{\text{Diode}}$ ).

Therefore, in Fig. 8(b), for example, the voltage  $u_{AB}$  across the DUT is initially at the dc-link voltage level, hence the output capacitance of the DUT and the switch  $S_1$  is small compared to the one of  $S_2$  and only a small part of the inductor current  $i_L$  is initially flowing through the DUT's output capacitance. On the other hand, when  $u_{AB}$  is small, the major part of  $i_L$  is charging the DUT's output capacitance, as shown in Fig. 8(c).

For the actual measurement of the CDL, the same measurement principle as described for the SSL measurements is used (cf., Section II). The DUT is mounted on a thermally insulated brass block and the measurement temperature range is again 30°C–40°C unless otherwise noted. However, in order to identify which component, i.e., the SiC-MOSFET or the JBS diode, is causing the CDL, two different types of modules, a Co-Pack module containing a SiC-MOSFET with a JBS diode and a module with only a JBS diode, are tested [cf., Fig. 1(a) and (b) and Fig. 7(b) and (c)].

## B. Measurement Results

In Fig. 10, the results of the CDL measurements obtained with the Co-Pack module [denoted as CDL, 30–40°C (MOSFET + Diode)] according to Fig. 10 are shown together with the results of the SSL measurements for dc-link voltages of 4–7 kV and currents between 2.5 and 15 A. Surprisingly, at low currents the CDL and the SSL are almost identical and with higher currents, the losses drift apart from each other as indicated with the gray areas. This residual loss fraction, which is the loss difference between the SSL and the CDL, should actually correspond to the turn-off losses caused in the MOSFET-channel due to the overlapping of the voltage and current transients. Unexpectedly, the residual losses are increasing with decreasing dc-link voltage. Actually, the residual losses should be independent from the applied dc-link voltage, since on one hand the MOSFET-channel losses are only generated in the initial period of the switching transition where the MOSFET-channel has not yet completely stopped conducting, and on the other hand the  $du/dt$  only depends on the switched current, which

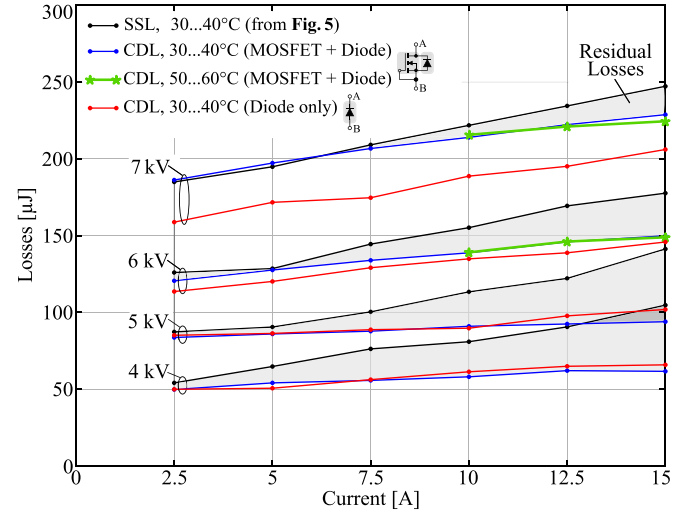


Fig. 10. Measured CDL of the Co-Pack module and the separate JBS diode together with the corresponding SSL curves from Fig. 5. Note that measurements obtained at 30°C–40°C and 50°C–60°C are almost identical, i.e., the CDL are independent of the junction temperature.

consequently results in the same overlapping of voltage and current transients. It is reasonable that the MOSFET-channel losses increase with increasing switched current; however, in this case typically the total SSL would not anymore increase linearly but rather disproportionately as shown in Fig. 5 for a turn-off resistor of  $R_{\text{off}} = 15 \Omega$ . Therefore, it is presumed that the deviation between the measured SSL and the CDL is caused by the introduced (and indispensable) damping resistor  $R_D$ , which on one hand distorts the current waveform in the DUT—especially at higher current ratings or  $du/dt$ -values—and on the other hand the voltage across  $R_D$  (worst case is  $20 \Omega \cdot 15 \text{ A} = 300 \text{ V}$ ) becomes more dominant at lower dc-link voltages. This means that, due to the linear slope of the SSL with respect to switched current and the fact that the CDL and the SSL are equal at low current, the two measurements should effectively be more or less equal at higher current ratings. Notwithstanding the above, the key message of the measurement results is that the SSL are almost exclusively originating from the charging/discharging of the DUT's output capacitance and not from the overlapping of the voltage and current transients. Consequently, the CDL constitute a lower limit for the SSL, independently of the gate driver performance and the packaging inductances of the device, which only affect the already comparably low turn-off losses.

Additionally, the CDL would also directly affect the performance of resonant dc-link inverters, which achieve zero voltage switching (ZVS) by forcing the drain–source voltage of the MOSFETs to zero during the current commutation by means of introducing a resonance to the dc-link capacitor [26]–[28]. Thereby, although the commutation of the load current within one MOSFET half-bridge is performed under zero voltage (and can be assumed as lossless), the output capacitances of the MOSFETs still have to be charged and discharged, leading to certain  $du/dt$  dependent CDL, which have to be taken into account.

Furthermore, for the analysis of the temperature dependence of the CDL, the measurements were also conducted at a higher

brass block temperature range of 50°C–60°C [cf., Fig. 10, denoted as CDL, 50–60°C (MOSFET + Diode) according to Fig. 10]. As can be seen, the measurements obtained at 30°C–40°C and 50°C–60°C are almost identical. Hence, the CDL, and since these losses account for the majority of the SSL, also the SSL can be assumed to be independent from the chip temperature, as it is also the case for the hard-switching losses measured in [29]–[31].

In order to get a better idea about the resulting losses of the underlying application, the CDL, which in this case more or less correspond to the SSL, are set in relation to the stored energy in the parasitic output capacitance. For the tested 10-kV SiC Co-Pack modules, the SSL approximately correspond to 5% – 10% of the stored energy within the measured current and voltage range, which underpins the outstanding switching characteristics of these 10-kV SiC devices and enables the use of comparably high switching frequencies in soft-switched applications.

It is now clear that the CDL of the 10-kV SiC Co-Pack modules at hand are responsible for the largest share of the SSL. However, the question in which component, i.e., the SiC-MOSFET or the JBS diode, the CDL are generated, remains. Therefore, besides the Co-Pack module also a separate discrete JBS diode in an identical package is tested [cf., Fig. 7(c)]. The corresponding CDL measurements are also shown in Fig. 10 [denoted as CDL, 30–40°C (Diode only) according to Fig. 10]. For dc-link voltages of 4–6 kV, the CDL of the diode are more or less equal to the losses measured with the Co-Pack module. At a dc-link voltage of 7 kV, however, the measured CDL are slightly lower compared to the losses of the Co-Pack module, which means that the MOSFET starts to contribute to the CDL. Nevertheless, based on these measurements, the majority of the CDL, and consequently also of the SSL, have to be attributed to the JBS diode and surprisingly not to the SiC-MOSFET. Unfortunately, the CDL and their distribution among the JBS diode and the MOSFET cannot be estimated by the measurement of their output capacitances, since, although the capacitance of the JBS diode is only two times larger than the output capacitance of the MOSFET (cf., Fig. 9 at higher voltages), almost the entire CDL are generated by the JBS diode. Therefore, it has to be assumed that the CDL loss mechanisms are not the same in the JBS diode and the MOSFET.

As a consequence, in order to strongly reduce the SL in converter systems employing soft-switching techniques, the JBS diode could be omitted and instead the body diode of the SiC-MOSFET could be used. Even though the body diode might have a much higher forward voltage drop, the additional CL in the short dead time interval are relatively small compared to the saved SSL. Unfortunately, since a module with a separate SiC-MOSFET was not available, the authors did not have the opportunity to confirm this statement by experimental results.

## V. CONCLUSION

In this paper, a novel accurate calorimetric method for the measurement of SSL of a 10-kV SiC MOSFET is presented. As shown in the literature, electrical measurement methods, such

as the double pulse test, can lead to large measurement errors, and thus are unsuitable for the characterization of the considered 10-kV SiC MOSFET and other fast-switching devices. On the other hand, with calorimetric measurement methods, the total semiconductor losses can be measured accurately. However, the calorimetric methods presented in literature so far were not able to separate the SL from the CL without calculations of, e.g., the CL, which could result again in certain measurement errors. This disadvantage is eliminated by the proposed measurement method, where an additional switch is introduced and which in combination with a novel modulation scheme enables to measure the CL and the SL separately. The error analysis for the proposed measurement method shows that the worst case error is 15%, which is a factor of 10–20, more accurate than the accuracy obtained with the double pulse method. Based on the proposed measurement method, the SSL of the 10-kV SiC MOSFET are examined for different dc-link voltages, switched currents, and gate resistors.

Additional CDL measurements revealed that the charging and discharging process of the output capacitances of the MOSFET and antiparallel JBS diode generate the largest part of the SSL. Furthermore, by testing a Co-Pack module (consisting of a 10-kV SiC-MOSFET in combination with a 10-kV JBS diode) and a separate 10-kV JBS diode module, it could be identified that the major part of the CDL and hence a major part of the SSL has to be attributed to the JBS diode and surprisingly not to the SiC-MOSFET.

Compared to the hard-switching losses, the SSL are almost 100 times lower, which enables a higher converter performance. However, the SSL are still relevant in comparison to the CL and therefore have to be considered in the converter design, especially for applications utilizing high switching frequencies.

## ACKNOWLEDGMENT

The authors would like to thank Wolfspeed, a Cree Company, for granting access to prototype 10-kV SiC MOSFETs and diodes. This research project is part of the National Research Programme “Energy Turnaround” (NRP 70) of the Swiss National Science Foundation. Further information on the National Research Programme can be found at [www.nrp70.ch](http://www.nrp70.ch).

## REFERENCES

- [1] M. Pahlevani, S. Eren, A. Bakhshai, and P. Jain, “A series-parallel current-driven full-bridge DC/DC converter,” *IEEE Trans. Power Electron.*, vol. 31, no. 2, pp. 1275–1293, Feb. 2016.
- [2] R. W. Erickson and D. Maksimovic, *Fundamentals of Power Electronics* (Soft Switching), 2nd ed. Berlin, Germany: Springer, 2001, ch. 20.
- [3] A. Safaei, P. Jain, and A. Bakhshai, “A ZVS pulsedwidth modulation full-bridge converter with a low-rms-current resonant auxiliary circuit,” *IEEE Trans. Power Electron.*, vol. 31, no. 6, pp. 4031–4047, Jun. 2016.
- [4] A. Anurag, S. Bal, and B. ChittiBabu, “A detailed comparative analysis between two soft switching techniques used in PV applications,” in *Proc. IEEE India Int. Conf.*, Kochi, India, 2012, pp. 1234–1239.
- [5] Z. Guo, K. Sun, and D. Sha, “Improved ZVS three-level DC-DC converter with reduced circulating loss,” *IEEE Trans. Power Electron.*, vol. 31, no. 9, pp. 6394–6404, Sep. 2016.
- [6] F. Jauch and J. Biela, “Combined phase-shift and frequency modulation of a dual-active-bridge AC-DC converter with PFC,” *IEEE Trans. Power Electron.*, vol. 31, no. 12, pp. 8387–8397, Dec. 2016.

- [7] C. Marxgut, F. Krismer, D. Bortis, and J. W. Kolar, "Ultraflat Interleaved Triangular Current Mode (TCM) Single-Phase PFC Rectifier," *IEEE Trans. Power Electron.*, vol. 29, no. 2, pp. 873–882, Feb. 2014.
- [8] D. Bortis, D. Neumayr, and J. W. Kolar, " $\eta/\rho$ -Pareto optimization and comparative evaluation of inverter concepts considered for the GOOGLE little box challenge," in *Proc. IEEE Workshop Control Model. Power Electron.*, Trondheim, Norway, 2016, pp. 1–11.
- [9] H. F. Xiao, L. Zhang, and Y. Li, "A zero-voltage-transition HERIC-type transformerless photovoltaic grid-connected inverter," *IEEE Trans. Ind. Electron.*, vol. 64, no. 2, pp. 1222–1232, Feb. 2017.
- [10] R. Callanan *et al.*, "Recent progress in SiC DMOSFETs and JBS diodes at cree," in *Proc. Ann. Conf. IEEE Ind. Electron. Soc.*, Orlando, FL, USA, 2008, pp. 2885–2890.
- [11] D. Han, J. Noppakunkajorn, and B. Sarlioglu, "Efficiency comparison of SiC and Si-Based bidirectional DC–DC converters," in *Proc. IEEE Transp. Electricif. Conf. Expo.*, Detroit, MI, USA, 2013, pp. 1–7.
- [12] O. Deblecker, Z. De Greve, and C. Versele, "Evaluation of Power Loss and Mass Gains of SiC versus Si-Based Switch-Mode Power Supplies using a Multiobjective Optimization CAD Tool," in *Proc. 2014 Int. Symp. Power Electron., Electr. Drives, Autom. Motion*, Ischia, Italy, 2014, pp. 43–49.
- [13] R. M. Burkart and J. W. Kolar, "Comparative evaluation of SiC and Si PV inverter systems based on power density and efficiency as indicators of initial cost and operating revenue," in *Proc. IEEE Workshop Control Model. Power Electron.*, Salt Lake City, UT, USA, 2013.
- [14] J. Hu *et al.*, "Robustness and balancing of parallel-connected power devices: SiC versus CoolMOS," *IEEE Trans. Ind. Electron.*, vol. 63, no. 4, pp. 2092–2102, Apr. 2016.
- [15] D. Rothmund, D. Bortis, and J. W. Kolar, "Accurate transient calorimetric measurement of soft-switching losses of 10kV SiC MOSFETs," in *Proc. Int. Symp. Power Electron. Distrib. Gener. Syst.*, Vancouver, BC, Canada, 2016, pp. 1–10.
- [16] A. Tüysüz, R. Bosshard, and J. W. Kolar, "Performance comparison of a GaN GIT and a Si IGBT for high-speed drive applications," in *Proc. Int. Power Electron. Conf.*, Hiroshima, Japan, 2014, pp. 1904–1911.
- [17] L. Hoffmann, C. Gautier, S. Lefebvre, and F. Costa, "Optimization of the driver of GaN power transistors through measurement of their thermal behavior," *IEEE Trans. Power Electron.*, vol. 29, no. 5, pp. 2359–2366, May 2014.
- [18] D. Rothmund, G. Ortiz, T. Guillod, and J. W. Kolar, "10kV SiC-Based isolated DC–DC converter for medium voltage-connected solid-state transformers," in *Proc. IEEE Appl. Power Electron. Conf. (APEC)*, Charlotte, NC, USA, 2015, pp. 1096–1103.
- [19] D. Wang *et al.*, "A 10-kV/400-V 500-kVA electronic power transformer," *IEEE Trans. Ind. Electron.*, vol. 63, no. 11, pp. 6653–6663, Nov. 2016.
- [20] C. Gu, Z. Zheng, L. Xu, K. Wang, and Y. Li, "Modeling and control of a multiport power electronic transformer (PET) for electric traction applications," *IEEE Trans. Power Electron.*, vol. 31, no. 2, pp. 915–927, Feb. 2016.
- [21] D. Bortis, O. Knecht, D. Neumayr, and J. W. Kolar, "Comprehensive evaluation of GaN GIT in low- and high-frequency bridge leg applications," in *Proc. Int. Power Electron. Motion Control Conf.*, Hefei, China, 2016, pp. 21–30.
- [22] J. B. Fedison, M. Fornage, M. J. Harrison, and D. R. Zimmanck, "Coss related energy loss in power MOSFETs used in zero-voltage-switched applications," in *Proc. IEEE Appl. Power Electron. Conf. Expo.*, Fort Worth, TX, USA, 2014, pp. 150–156.
- [23] J. B. Casady, E. V. Brunt, G.-y. Wang, J. Richmond, S. T. Allen, and D. Grider, "New generation 10kV SiC power MOSFET and diodes for industrial applications," in *Proc. Conf. Power Convers. Intell. Motion*, Nuremberg, Germany, 2015, pp. 96–103.
- [24] J. B. Fedison and M. J. Harrison, "Coss Hysteresis in Advanced Superjunction MOSFETs," in *Proc. IEEE Appl. Power Electron. Conf.*, Long Beach, CA, USA, 2016, pp. 247–252.
- [25] J. Roig and F. Bauwens, "Origin of anomalous  $C_{oss}$  hysteresis in resonant converters with superjunction FETs," *IEEE Trans. Electron Devices*, vol. 62, no. 9, pp. 3092–3094, Sep. 2015.
- [26] S. Mandrek and P. J. Chrzan, "Quasi-resonant DC-link inverter with a reduced number of active elements," *IEEE Trans. Ind. Electron.*, vol. 54, no. 4, pp. 2088–2094, Aug. 2007.
- [27] P. Musznicki, M. Turzynski, and P. J. Chrzan, "Accurate modeling of quasi-resonant inverter fed IM drive," in *Proc. Annu. Conf. IEEE Ind. Electron. Soc. (IECON)*, Vienna, Austria, 2013, pp. 376–381.
- [28] N. Mohan, T. M. Undeland, and W. P. Robbins, "Resonant-DC-link inverters with zero-voltage switchings," in *Power Electronics: Converters, Applications, and Design*, 3rd ed. New York, NY, USA: Wiley, 2003, chs. 9–7, pp. 287–289.
- [29] S. Madhusoodhanan, K. Mainali, A. Tripathi, K. Vechalapu, and S. Bhattacharya, "Medium voltage ( $>2.3$  kV) high frequency three-phase two-level converter design and demonstration using 10 kV SiC MOSFETs for high speed motor drive applications," in *Proc. IEEE Appl. Power Electron. Conf. Expo.*, Long Beach, CA, USA, 2016, pp. 1497–1504.
- [30] J. Thoma, D. Chilachava, and D. Kranzer, "A highly efficient DC–DC-converter for medium-voltage applications," in *Proc. IEEE Int. Energy Conf.*, Dubrovnik, Croatia, 2014, pp. 140–144.
- [31] K. Vechalapu, S. Bhattacharya, E. V. Brunt, S.-h. Ryu, and D. Grider, "Comparative evaluation of 15 kV SiC MOSFET and 15 kV SiC IGBT for medium voltage converter under same dv/dt conditions," in *Proc. IEEE Energy Convers. Congr. Expo.*, Montreal, QC, Canada, 2015, pp. 927–934.



**Daniel Rothmund** (S'14) received the M.Sc. degree in electrical engineering and information technology from ETH Zurich, Zurich, Switzerland, in 2013, with focus on power electronics, high-voltage technology, and electric power systems. Since 2013, he has been working toward the Ph.D. degree in SiC-Based Medium-Voltage Solid-State-Transformer Concepts for Power Supply of 400 V DC Distribution Systems from Power Electronic Systems Laboratory, ETH Zurich.

His current research focuses on 10-kV silicon carbide based medium voltage to 400-V dc solid-state transformers and their optimization.



**Dominik Bortis** (M'08) received the M.Sc. degree in electrical engineering and the Ph.D. degree in 20 MW Halbleiter-Leistungsmodulator-System from Swiss Federal Institute of Technology (ETH) Zurich, Zurich, Switzerland, in 2005 and 2008, respectively.

From 2008 to 2011, he was a Postdoctoral Fellow and from 2011 to 2016 a Research Associate in the Power Electronic Systems Laboratory (PES), ETH Zurich, cosupervising Ph.D. students and leading industry research projects. Since January 2016, he is heading the newly established research group Advanced Mechatronic Systems, at PES, ETH Zurich.



**Johann Walter Kolar** (F'10) is a Fellow of the IEEE and received his Ph.D. degree (*summa cum laude*) from the Vienna University of Technology, Austria. He is currently a Full Professor and the Head of the Power Electronic Systems Laboratory at the Swiss Federal Institute of Technology (ETH) Zurich. He has published over 750 scientific papers in international journals and conference proceedings and has filed more than 140 patents. He received 25 IEEE Transactions and Conference Prize Paper Awards, the 2014 IEEE Power Electronics Society R. David

Middlebrook Achievement Award, the 2016 IEEE William E. Newell Power Electronics Award, the 2016 IEEE PEMC Council Award, and the ETH Zurich Golden Owl Award for excellence in teaching. The focus of his current research is on ultra-compact and ultra-efficient SiC and GaN converter systems, wireless power transfer, Solid-State Transformers, Power Supplies on Chip, as well as ultra-high speed and ultra-light weight drives, bearingless motors, and energy harvesting.